

Fundamental limits on the rate of bacterial cell division

³ **Nathan M. Belliveau^{†, 1}, Griffin Chure^{†, 2, 3}, Christina L. Hueschen⁴, Hernan G.
⁴ Garcia⁵, Jané Kondev⁶, Daniel S. Fisher⁷, Julie Theriot^{1, 8}, Rob Phillips^{2, 9, *}**

*For correspondence:

[†]These authors contributed equally to this work

⁵ ¹Department of Biology, University of Washington, Seattle, WA, USA; ²Division of
⁶ Biology and Biological Engineering, California Institute of Technology, Pasadena, CA,
⁷ USA; ³Department of Applied Physics, California Institute of Technology, Pasadena, CA,
⁸ USA; ⁴Department of Chemical Engineering, Stanford University, Stanford, CA, USA;
⁹ ⁵Department of Molecular Cell Biology and Department of Physics, University of
¹⁰ California Berkeley, Berkeley, CA, USA; ⁶Department of Physics, Brandeis University,
¹¹ Waltham, MA, USA; ⁷Department of Applied Physics, Stanford University, Stanford, CA,
¹² USA; ⁸Allen Institute for Cell Science, Seattle, WA, USA; ⁹Department of Physics,
¹³ California Institute of Technology, Pasadena, CA, USA; *Contributed equally

¹⁴

¹⁵ Abstract

¹⁶

¹⁷ Introduction

¹⁸ The range of bacterial growth rates is enormously diverse. In natural environments, some micro-
¹⁹ bial organisms might double only once per year while in comfortable laboratory conditions, growth
²⁰ can be rapid with several divisions per hour. This six order of magnitude difference illustrates the
²¹ intimate relationship between environmental conditions and the rates at which cells convert nu-
²² trients into new cellular material – a relationship that has remained a major topic of inquiry in
²³ bacterial physiology for over a century (*Jun et al., 2018*). As was noted by Jacques Monod, “the
²⁴ study of the growth of bacterial cultures does not constitute a specialized subject or branch of re-
²⁵ search, it is the basic method of Microbiology.” Those words ring as true today as they did when
²⁶ they were written 70 years ago. Indeed, the study of bacterial growth has undergone a molecular
²⁷ resurgence since many of the key questions addressed by the pioneering efforts in the middle of
²⁸ the last century can be revisited by examining them through the lens of the increasingly refined
²⁹ molecular census that is available for bacteria such as the microbial workhorse *Escherichia coli*. Sev-
³⁰ eral of the outstanding questions that can now be studied about bacterial growth include: what
³¹ sets the fastest time scale that bacteria can divide, and how is growth rate tied to the quality of the
³² carbon source. In this paper, we address these two questions from two distinct angles. First, as
³³ a result of an array of high-quality proteome-wide measurements of the *E. coli* proteome under a
³⁴ myriad of different growth conditions, we have a census that allows us to explore how the num-
³⁵ ber of key molecular players change as a function of growth rate. This census provides a window
³⁶ onto whether the processes they mediate such as molecular transport into the cells and molecular
³⁷ synthesis within cells can run faster. Second, because of our understanding of the molecular path-
³⁸ ways responsible for many of the steps in bacterial growth, we can also make order of magnitude
³⁹ estimates to infer the copy numbers that would be needed to achieve a given growth rate. In this
⁴⁰ paper, we pass back and forth between the analysis of a variety of different proteomic datasets and
⁴¹ order-of-magnitude estimations to determine possible molecular bottlenecks that limit bacterial

42 growth and to see how the growth rate varies in different carbon sources.

43 Specifically, we leverage a combination of *E. coli* proteomic data sets collected over the past
 44 decade using either mass spectrometry (*Schmidt et al., 2016; Peebo et al., 2015; Valgepea et al.,
 45 2013*) or ribosomal profiling (*Li et al., 2014*) across 31 unique growth conditions. Broadly speaking,
 46 we entertain several classes of hypotheses as are illustrated in **Figure 1**. First, we consider potential
 47 limits on the transport of nutrients into the cell. We address this hypothesis by performing an
 48 order-of-magnitude estimate for how many carbon, phosphorous, and sulfur atoms are needed to
 49 facilitate this requirement given a 5000 second division time. As a second hypothesis, we consider
 50 the possibility that there exists a fundamental limit on how quickly the cell can generate ATP. We
 51 approach this hypothesis from two angles, considering how many ATP synthase complexes must
 52 be needed to churn out enough ATP to power protein translation followed by an estimation of
 53 how many electron transport complexes must be present to maintain the proton motive force.
 54 A third class of estimates considers the need to maintain the size and shape of the cell through
 55 the construction of new lipids for the cell membranes as well as the glycan polymers which make
 56 up the rigid peptidoglycan. Our final class of hypotheses centers on the synthesis of a variety of
 57 biomolecules. Our focus is primarily on the stages of the central dogma as we estimate the number
 58 of protein complexes needed for DNA replication, transcription, and protein translation.

59 In broad terms, we find that the majority of these estimates are in close agreement with the
 60 experimental observations, with protein copy numbers apparently well-tuned for the task of cell
 61 doubling. This allows us to systematically scratch off the hypotheses diagrammed in **Figure 1** as
 62 setting possible speed limits. Ultimately, we find that protein translation (particularly the genera-
 63 tion of new ribosomes) acts as 1) a rate limiting step for the *fastest* bacterial division, and 2) the
 64 major determinant of bacterial growth across all nutrient conditions we have considered under
 65 steady state, exponential growth. This perspective is in line with the linear correlation observed
 66 between growth rate and ribosomal content (typically quantified through the ratio of RNA to pro-
 67 tein) for fast growing cells (*Scott et al., 2010*), but suggests a more prominent role for ribosomes
 68 in setting the doubling time across all conditions of nutrient limitation. Here we again leverage the
 69 quantitative nature of this data set and present a quantitative model of the relationship between
 70 the fraction of the proteome devoted to ribosomes and the speed limit of translation, revealing
 71 a fundamental tradeoff between the translation capacity of the ribosome pool and the maximal
 72 growth rate.

73 Uptake of Nutrients

74 In order to build new cellular mass, the molecular and elemental building blocks must be scav-
 75 enged from the environment in different forms. Carbon, for example, is acquired via the transport
 76 of carbohydrates and sugar alcohols with some carbon sources receiving preferential treatment
 77 in their consumption (*Monod, 1947*). Phosphorus, sulfur, and nitrogen, on the other hand, are
 78 harvested primarily in the forms of inorganic salts, namely phosphate, sulfate, and ammonia (*Jun
 79 et al., 2018; Assentoft et al., 2016; Stasi et al., 2019; Antonenko et al., 1997; Rosenberg et al., 1977;
 80 Willsky et al., 1973*). All of these compounds have different permeabilities across the cell mem-
 81 brane and most require some energetic investment either via ATP hydrolysis or through the pro-
 82 ton electrochemical gradient to bring the material across the hydrophobic cell membrane. Given
 83 the diversity of biological transport mechanisms and the vast number of inputs needed to build a
 84 cell, we begin by considering transport of some of the most important cellular ingredients: carbon,
 85 nitrogen, oxygen, hydrogen, phosphorus, and sulfur.

86 The elemental composition of *E. coli* has received much quantitative attention over the past
 87 half century (*Neidhardt et al., 1991; Taymaz-Nikerel et al., 2010; Heldal et al., 1985; Bauer and
 88 Ziv, 1976*), providing us with a starting point for estimating the copy numbers of various trans-
 89 porters. While there is some variability in the exact elemental percentages (with different uncer-
 90 tainties), we can estimate that the dry mass of a typical *E. coli* cell is \approx 45% carbon (BNID: 100649,
 91 *Milo et al. (2010)*), \approx 15% nitrogen (BNID: 106666, *Milo et al. (2010)*), \approx 3% phosphorus (BNID:

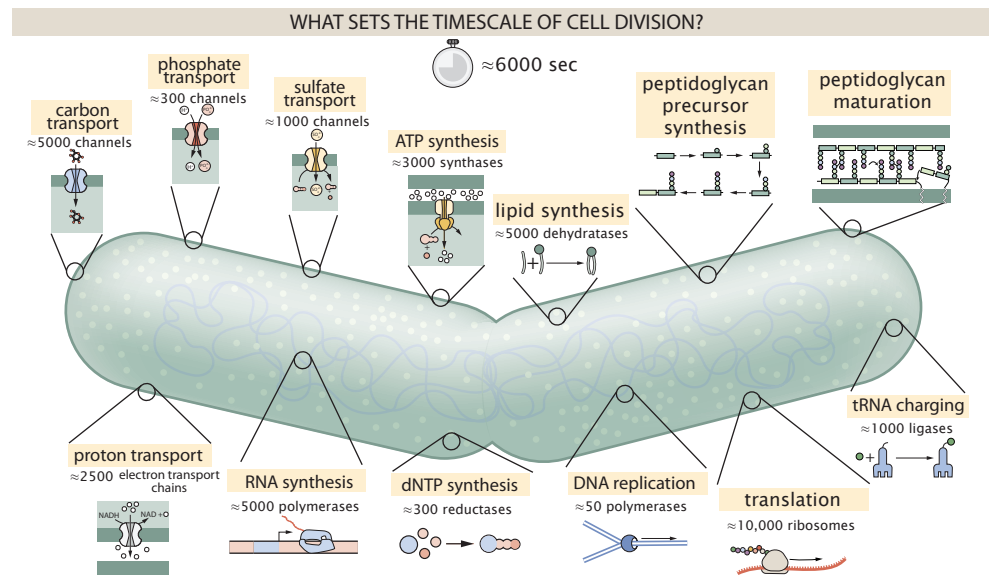


Figure 1. Transport and synthesis processes necessary for cell division. We consider an array of processes necessary for a cell to double its molecular components. Such processes include the transport of carbon across the cell membrane, the production of ATP, and fundamental processes of the central dogma namely RNA, DNA, and protein synthesis. A schematic of each synthetic or transport category is shown with an approximate measure of the complex abundance at a growth rate of 0.5 per hour. In this work, we consider a standard bacterial division time of ≈ 5000 sec.

92 100653, *Milo et al. (2010)*), and 1% sulfur (BNID: 100655, *Milo et al. (2010)*). In the coming para-
 93 graphs, we will engage in a dialogue between back-of-the-envelope estimates for the numbers of
 94 transporters needed to facilitate these chemical stoichiometries and the experimental proteomic
 95 measurements of the biological reality. Such an approach provides the opportunity to test if our
 96 biological knowledge is sufficient to understand the scale at which these complexes are produced.
 97 Specifically, we will make these estimates considering a modest doubling time of 5000 s, a growth
 98 rate of $\approx 0.5 \text{ hr}^{-1}$, the range in which the majority of the experimental measurements reside.

99 Carbon Transport

100 We begin with the most abundant element by mass, carbon. Using $\approx 0.3 \text{ pg}$ as the typical *E. coli*
 101 dry mass (BNID: 103904, *Milo et al. (2010)*), we estimate that $\approx 10^{10}$ carbon atoms must be brought
 102 into the cell in order to double all of the carbon-containing molecules (*Figure 2(A, top)*). Typical
 103 laboratory growth conditions, such as those explored in the aforementioned proteomic data sets,
 104 provide carbon as a single class of sugar such as glucose, galactose, or xylose to name a few. *E. coli*
 105 has evolved myriad mechanisms by which these sugars can be transported across the cell
 106 membrane. One such mechanism of transport is via the PTS system which is a highly modular
 107 system capable of transporting a diverse range of sugars (*Escalante et al., 2012*). The glucose-
 108 specific component of this system transports ≈ 200 glucose molecules per second per channel
 109 (BNID: 114686, *Milo et al. (2010)*). Making the assumption that this is a typical sugar transport rate,
 110 coupled with the need to transport 10^{10} carbon atoms, we arrive at the conclusion that on the
 111 order of 1,000 transporters must be expressed in order to bring in enough carbon atoms to divide
 112 in 6,000 s, diagrammed in the top panel of *Figure 2(A)*. This estimate, along with the observed
 113 average number of carbohydrate transporters present in the proteomic data sets (*Schmidt et al.,*
 114 *2016; Peebo et al., 2015; Valgepea et al., 2013; Li et al., 2014*), is shown in *Figure 2(A)*. While we
 115 estimate 1,000 transporters are needed, the data reveals that at a division time of ≈ 5000 s there is
 116 nearly a ten-fold excess of transporters. Furthermore, the data illustrates that the average number
 117 of carbohydrate transporters present is largely-growth rate independent.

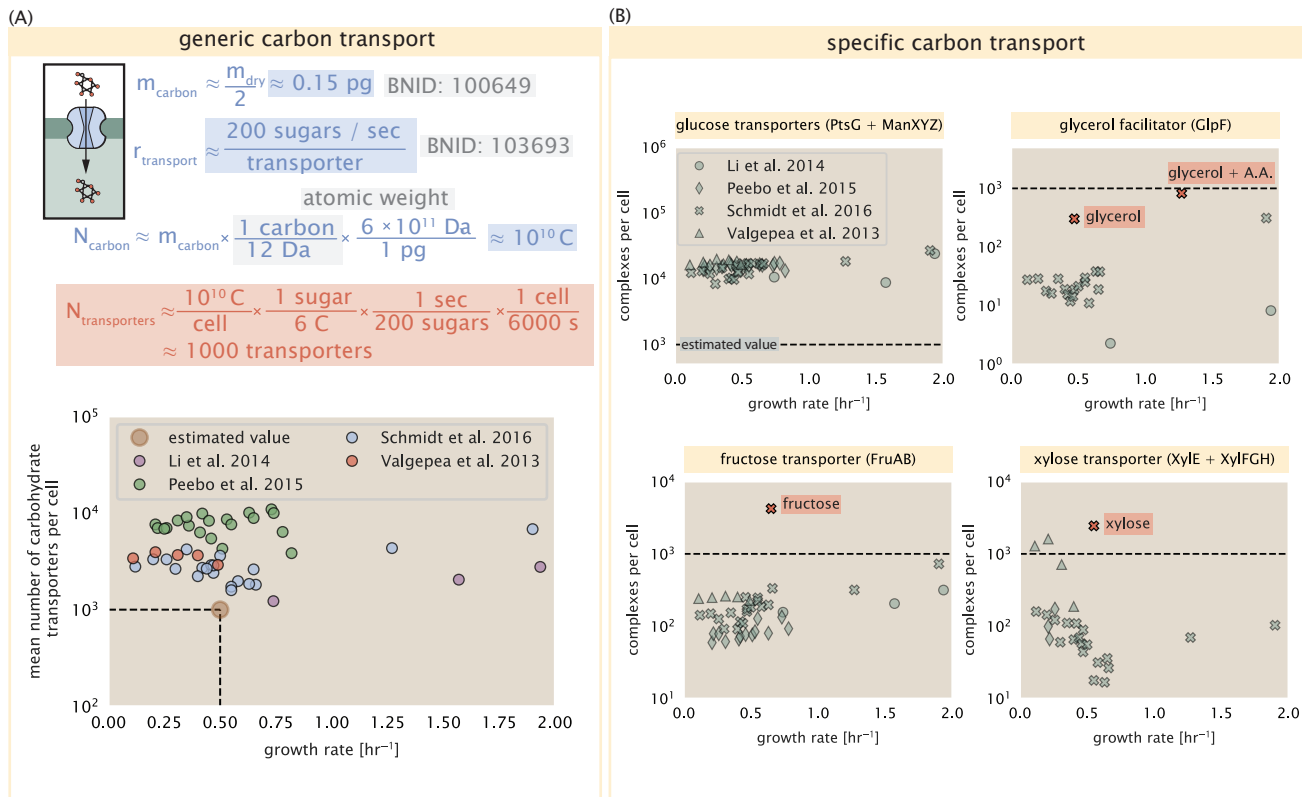


Figure 2. The abundance of carbon transport systems across growth rates. (A) A simple estimate for the minimum number of generic carbohydrate transport systems (top) assumes $\approx 10^{10}$ C are needed to complete division, each transported sugar contains ≈ 6 C, and each transporter conducts sugar molecules at a rate of ≈ 200 per second. Bottom plot shows the estimated number of transporters needed at a growth rate of ≈ 0.5 per hr (light-brown point and dashed lines). Colored points correspond to the mean number of carbohydrate transporters for different growth conditions across different published datasets. (B) The abundance of various specific carbon transport systems plotted as a function of the population growth rate. Red points and red-highlighted text indicate conditions in which the only source of carbon in the growth medium induces expression of the transport system.

118 The estimate presented in **Figure 2(A)** neglects any specifics of the regulation of carbon trans-
 119 port system and presents a data-averaged view of how many carbohydrate transporters are present
 120 on average. Using the diverse array of growth conditions explored in the proteomic data sets,
 121 we can explore how individual carbon transport systems depend on the population growth rate.
 122 In **Figure 2(B)**, we show the total number of carbohydrate transporters specific to different car-
 123 bon sources. A striking observation, shown in the top-left plot of **Figure 2(B)**, is the constancy
 124 in the expression of the glucose-specific transport systems (the PtsG enzyme of the PTS system
 125 and the glucose-transporting ManXYZ complex). Additionally, we note that the total number of
 126 glucose-specific transporters is tightly distributed $\approx 10^4$ per cell, an order of magnitude beyond
 127 the estimate shown in **Figure 2(A)**. This illustrates that *E. coli* maintains a substantial number of
 128 complexes present for transporting glucose which is known to be the preferential carbon source
 129 (*Monod, 1947; Liu et al., 2005; Aidelberg et al., 2014*).

130 It is now understood that a large number of metabolic operons are regulated with dual-input
 131 logic gates that are only expressed when glucose concentrations are low (mediated by cyclic-AMP
 132 receptor protein CRP) and the concentration of other carbon sources are elevated (*Gama-Castro*
 133 *et al., 2016; Zhang et al., 2014b*). A famed example of such dual-input regulatory logic is in the regu-
 134 lation of the *lac* operon which is only natively activated in the absence of glucose and the presence
 135 of allolactose, an intermediate in lactose metabolism (*Jacob and Monod, 1961*), though we now
 136 know of many other such examples (*Ireland et al., 2020; Gama-Castro et al., 2016; Belliveau et al.,*
 137 *2018*). This illustrates that once glucose is depleted from the environment, cells have a means to
 138 dramatically increase the abundance of the specific transporter needed to digest the next sugar
 139 that is present. Several examples of induced expression of specific carbon-source transporters
 140 are shown in **Figure 2(B)**. Points colored in red (labeled by red text-boxes) correspond to growth
 141 conditions in which the specific carbon source (glycerol, xylose, or fructose) is present. These plots
 142 show that, in the absence of the particular carbon source, expression of the transporters is main-
 143 tained on the order of $\sim 10^2$ per cell. However, when induced, the transporters become highly-
 144 expressed and are present on the order of $\sim 10^4$ per cell, which exceeds the generic estimation given
 145 in **Figure 2(A)**. Together, this generic estimation and the specific examples of induced expression
 146 suggest that transport of carbon across the cell membrane, while critical for growth, is not the
 147 rate-limiting step of cell division.

148 In the context of speeding up growth, one additional limitation is the fact that the cell's inner
 149 membrane is occupied by a multitude of other membrane proteins. Considering a rule-of-thumb
 150 for the surface area of *E. coli* of about $6 \mu\text{m}^2$ (BNID: 101792, *Milo et al. (2010)*), we expect an areal
 151 density for 1,000 transporters to be approximately 200 transporters/ μm^2 . For a glucose trans-
 152 porter occupying about $50 \text{ nm}^2/\text{dimer}$, this amounts to about only 1 percent of the total inner
 153 membrane (*Szenk et al., 2017*). In addition, bacterial cell membranes typically have densities of
 154 10^5 proteins/ μm^2 (*Phillips, 2018*), implying that the cell could accommodate more transporters if
 155 it were rate limiting.

156 **Phosphorus and Sulfur Transport**

157 We now turn our attention towards other essential elements, namely phosphorus and sulfur. Phos-
 158 phorus is critical to the cellular energy economy in the form of high-energy phosphodiester bonds
 159 making up DNA, RNA, and the NTP energy pool as well as playing a critical role in the post-translational
 160 modification of proteins and defining the polar-heads of lipids. In total, phosphorus makes up
 161 $\approx 3\%$ of the cellular dry mass which in typical experimental conditions is in the form of inorganic
 162 phosphate. The cell membrane has remarkably low permeability to this highly-charged and critical
 163 molecule, therefore requiring the expression of active transport systems. In *E. coli*, the proton elec-
 164 trochemical gradient across the inner membrane is leveraged to transport inorganic phosphate
 165 into the cell (*Rosenberg et al., 1977*). Proton-solute symporters are widespread in *E. coli* (*Ramos and*
 166 *Kaback, 1977; Booth et al., 1979*) and can have rapid transport rates of 50 molecules per second
 167 for sugars and other solutes (BNID: 103159; 111777, *Milo et al. (2010)*). In *E. coli* the PitA phosphate

168 transport system has been shown to very tightly coupled with the proton electrochemical gradient
 169 with a 1:1 proton:phosphate stoichiometric ratio (*Harris et al., 2001; Feist et al., 2007*). Illustrated
 170 in *Figure 3(A)*, we can estimate that ≈ 300 phosphate transporters are necessary to maintain an
 171 $\approx 3\%$ dry mass with a 6,000 s division time. This estimate is again satisfied when we examine the
 172 observed copy numbers of PitA in proteomic data sets (plot in *Figure 3(A)*). While our estimate is
 173 very much in line with the observed numbers, we emphasize that this is likely a slight over estimate
 174 of the number of transporters needed as there are other phosphorous scavenging systems, such
 175 as the ATP-dependent phosphate transporter Pst system which we have neglected.

176 Satisfied that there are a sufficient number of phosphate transporters present in the cell, we
 177 now turn to sulfur transport as another potentially rate limiting process. Similar to phosphate,
 178 sulfate is highly-charged and not particularly membrane permeable, requiring active transport.
 179 While there exists a H⁺/sulfate symporter in *E. coli*, it is in relatively low abundance and is not well
 180 characterized (*Zhang et al., 2014a*). Sulfate is predominantly acquired via the ATP-dependent ABC
 181 transporter CysUWA system which also plays an important role in selenium transport (*Sekowska
 182 et al., 2000; Sirko et al., 1995*). While specific kinetic details of this transport system are not readily
 183 available, generic ATP transport systems in prokaryotes transport on the order of 1 to 10 molecules
 184 per second (BNID: 109035, *Milo et al. (2010)*). Combining this generic transport rate, measurement
 185 of sulfur comprising 1% of dry mass, and a 6,000 second division time yields an estimate of \approx
 186 1000 CysUWA complexes per cell (*Figure 3(B)*). Once again, this estimate is in notable agreement
 187 with proteomic data sets, suggesting that there are sufficient transporters present to acquire the
 188 necessary sulfur. In a similar spirit of our estimate of phosphorus transport, we emphasize that
 189 this is likely an overestimate of the number of necessary transporters as we have neglected other
 190 sulfur scavenging systems that are in lower abundance.

191 Nitrogen Transport

192 Finally, we turn to nitrogen transport as the last remaining transport system highlighted in *Fig-
 193 ure 1*. Unlike phosphate, sulfate, and various sugar molecules, nitrogen in the form of ammonia
 194 can readily diffuse across the cell membrane and has a permeability on par with water ($\approx 10^5$ nm/s,
 195 BNID:110824 *Milo et al. (2010)*). In particularly nitrogen-poor conditions, *E. coli* expresses a trans-
 196 porter (AmtB) which appears to aid in nitrogen assimilation, though the mechanism and kinetic
 197 details of transport is still a matter of debate (*van Heeswijk et al., 2013; Khademi et al., 2004*). Be-
 198 yond ammonia, another plentiful source of nitrogen come in the form of glutamate, which has its
 199 own complex metabolism and scavenging pathways. However, nitrogen is plentiful in the growth
 200 conditions examined in this work, permitting us to neglect nitrogen transport as a potential rate
 201 limiting process in cell division.

202 Function of the Central Dogma

203 Up to this point, we have considered a variety of transport and biosynthetic processes that are
 204 critical to acquiring and generating new cell mass. While there are of course many other metabolic
 205 processes we could consider and perform estimates of (such as the components of fermentative
 206 versus aerobic respiration), we now turn our focus to some of the most central processes which
 207 must be undertaken irrespective of the growth conditions – the processes of the central dogma.

208 DNA

209 Most bacteria (including *E. coli*) harbor a single, circular chromosome and can have extra-chromosomal
 210 plasmids up to ~ 100 kbp in length. We will focus our quantitative thinking solely on the chromo-
 211 some of *E. coli* which harbors ≈ 5000 genes and $\approx 5 \times 10^6$ base pairs. To successfully divide and
 212 produce viable progeny, this chromosome must be faithfully replicated and segregated into each
 213 nascent cell. We again rely on the near century of literature in molecular biology to provide some
 214 insight on the rates and mechanics of the replicative feat as well as the production of the required
 215 starting materials, dNTPs.

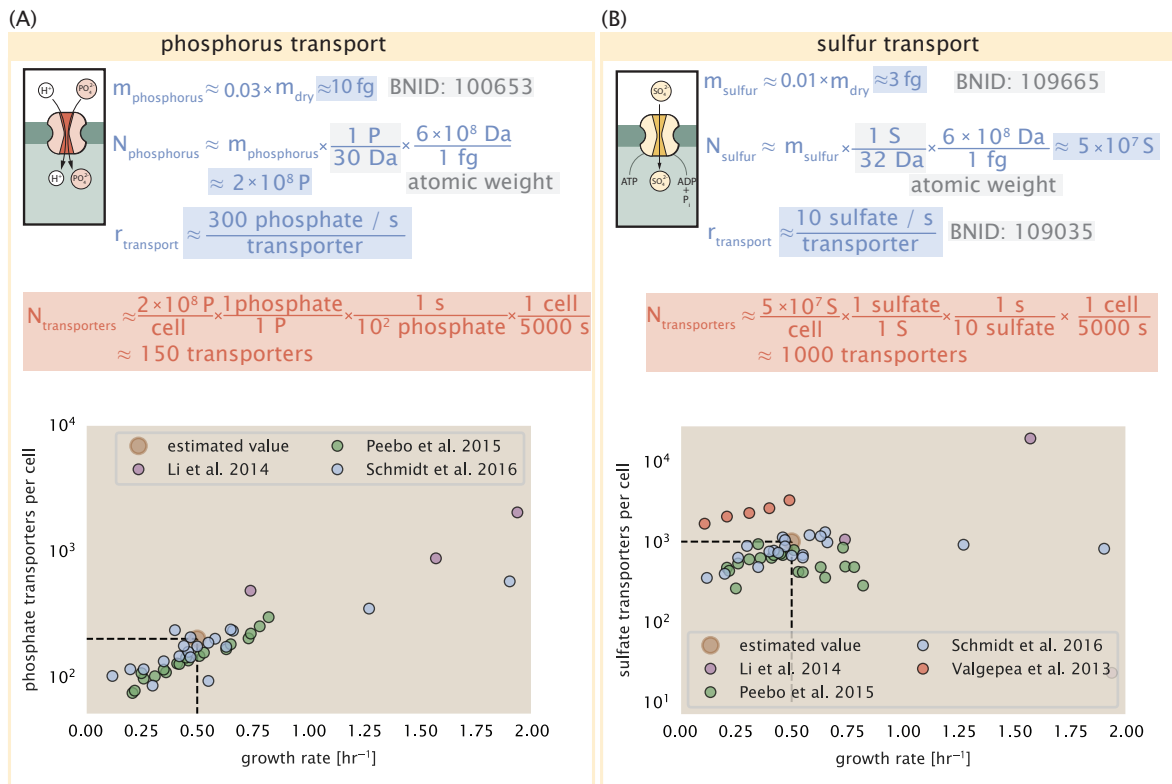


Figure 3. Estimates and measurements of phosphate and sulfate transport systems as a function of growth rate. (A) Estimate for the number of PitA phosphate transport systems needed to maintain a 3% phosphorus *E. coli* dry mass. Points in plot correspond to the total number of PitA transporters per cell. (B) Estimate of the number of CysUWA complexes necessary to maintain a 1% sulfur *E. coli* dry mass. Points in plot correspond to average number of CysUWA transporter complexes that can be formed given the transporter stoichiometry [CysA]₂[CysU][CysW][Sbp/CysP].

216 dNTP synthesis

217 We begin our exploration DNA replication by examining the production of the deoxyribonucleotide
 218 triphosphates (dNTPs). The four major dNTPs (dATP, dTTP, dCTP, and dGTP) are synthesized *de*
 219 *novo* in separate pathways, requiring different building blocks. However, a critical step present in
 220 all dNTP synthesis pathways is the conversion from ribonucleotide to deoxyribonucleotide via the
 221 removal of the 3' hydroxyl group of the ribose ring (Rudd *et al.*, 2016). This reaction is mediated
 222 by a class of enzymes termed ribonucleotide reductases, of which *E. coli* possesses two aerobically
 223 active complexes (termed I and II) and a single anaerobically active enzyme. Due to their peculiar
 224 formation of a radical intermediate, these enzymes have received much biochemical, kinetic, and
 225 structural characterization. One such work (Ge *et al.*, 2003) performed a detailed *in vitro* measure-
 226 ment of the steady-state kinetic rates of these complexes, revealing a turnover rate of ≈ 10 dNTP
 227 per second.

228 Since this reaction is central to the synthesis of all dNTPs, it is reasonable to consider the abun-
 229 dance of these complexes is a measure of the total dNTP production in *E. coli*. Illustrated schemati-
 230 cally in **Figure 4** (A), we consider the fact that to replicate the cell's genome, on the order of $\approx 10^7$
 231 dNTPs must be synthesized. Assuming a production rate of 10 per second per ribonucleotide
 232 reductase complex and a cell division time of 6000 seconds, we arrive at an estimate of ≈ 150 com-
 233 plexes needed per cell. As shown in the bottom panel of **Figure 4** (A), this estimate agrees with the
 234 experimental measurements of these complexes abundances within $\approx 1/2$ an order of magnitude.

235 Recent work has revealed that during replication, the ribonucleotide reductase complexes co-
 236 alesce to form discrete foci colocalized with the DNA replisome complex (Sánchez-Romero *et al.*,
 237 2011). This is particularly pronounced in conditions where growth is slow, indicating that spatial
 238 organization and regulation of the activity of the complexes plays an important role.

239 DNA Replication

240 We now turn our focus to the integration of these dNTP building blocks into the replicated chromo-
 241 some strand via the DNA polymerase. Replication is initiated at a single region of the chromosome
 242 termed the *oriC* locus at which a pair of DNA polymerases bind and begin their high-fidelity repli-
 243 cation of the genome in opposite directions. Assuming equivalence between the two replication
 244 forks, this means that the two DNA polymerase complexes (termed replisomes) meet at the mid-
 245 way point of the circular chromosome termed the *ter* locus. The kinetics of the five types of DNA
 246 polymerases (I – V) have been intensely studied, revealing that DNA polymerase III performs the
 247 high fidelity processive replication of the genome with the other "accessory" polymerases playing
 248 auxiliary roles (Fijalkowska *et al.*, 2012). *In vitro* measurements have shown that DNA Polymerase
 249 III copies DNA at a rate of ≈ 600 nucleotides per second (BNID: 104120, Milo *et al.* (2010)). Therefore,
 250 to replicate a single chromosome, two DNA polymerases replicating at their maximal rate would
 251 copy their entire genome in ≈ 4000 s. Thus, with a division time of 5000 s (our "typical" growth rate
 252 for the purposes of this work), there is sufficient time for a pair of DNA polymerase III complexes to
 253 replicate the entire genome. However, this estimate implies that 4000 s would be the upper-limit
 254 time scale for bacterial division which is at odds with the familiar 20 minute (1200 s) doubling time
 255 of *E. coli* in rich medium.

256 It is well known that *E. coli* can parallelize its DNA replication such that multiple chromosomes
 257 are being replicated at once, with as many as 10 - 12 replication forks at a given time (Bremer
 258 and Dennis, 2008; Si *et al.*, 2017). Thus, even in rapidly growing cultures, we expect only a few
 259 polymerases (≈ 10) are needed to replicate the chromosome per cell doubling. However, as shown
 260 in **Figure 4**(B), DNA polymerase III is nearly an order of magnitude more abundant. This
 261 discrepancy can be understood by considering its binding constant to DNA. DNA polymerase III is
 262 highly processive, facilitated by a strong affinity of the complex to the DNA. *In vitro* biochemical
 263 characterization has quantified the K_D of DNA polymerase III holoenzyme to single-stranded and
 264 double-stranded DNA to be 50 and 200 nM, respectively (Ason *et al.*, 2000). The bottom plot in
 265 **Figure 4** (B) shows that the concentration of the DNA polymerase III across all data sets and growth

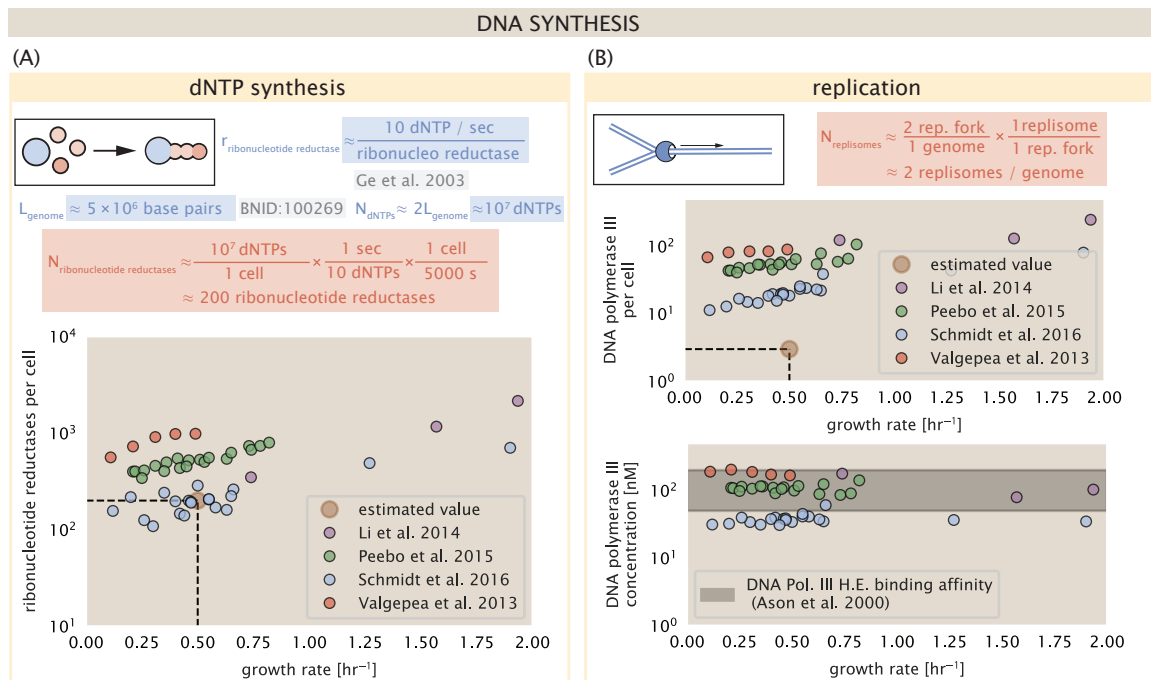


Figure 4. Complex abundance estimates for dNTP synthesis and DNA replication. (A) Estimate of the number of ribonucleotide reductase enzymes needed to facilitate the synthesis of $\approx 10^7$ dNTPs over the course of a 6000 second generation time. Points in the plot correspond to the total number of ribonucleotide reductase I ($[NrdA]_2[NrdB]_2$) and ribonucleotide reductase II ($[NrdE]_2[NrdF]_2$) complexes. (B) An estimate for the minimum number of DNA polymerase holoenzyme complexes needed to facilitate replication of a single genome. Points in the top plot correspond to the total number of DNA polymerase III holoenzyme complexes ($[DnaE]_3[DnaQ]_3[HolE]_3[DnaX]_5[HolB][HolA][DnaN]_4[HolC]_4[HolD]_4$) per cell. Bottom plot shows the effective concentration of DNA polymerase III holoenzyme given cell volumes calculated from the growth rate as in *Si et al. (2019)* (See Appendix Section 4).

266 conditions is within this range. Thus, while the copy number of the DNA polymerase III is in excess
 267 of the strict number required to replicate the genome, its copy number appears to vary such that its
 268 concentration is approximately equal to the dissociation constant to the DNA. While the processes
 269 regulating the initiation of DNA replication are complex and involve more than just the holoenzyme,
 270 these data indicate that the kinetics of replication rather than the explicit copy number of the DNA
 271 polymerase III holoenzyme is the more relevant feature of DNA replication to consider. In light
 272 of this, the data in **Figure 4(B)** suggests that for bacteria like *E. coli*, DNA replication does not represent a rate-limiting step in cell division. However, it is worth noting that for bacterium like *C. crescentus* whose chromosomal replication is initiated only once per cell cycle (*Jensen et al., 2001*), the time to double their chromosome likely represents an upper limit to their growth rate.

276 RNA Synthesis

277 With the machinery governing the replication of the genome accounted for, we now turn our attention
 278 to the next stage of the central dogma – the transcription of DNA to form RNA. We primarily
 279 consider three major groupings of RNA, namely the RNA associated with ribosomes (rRNA), the
 280 RNA encoding the amino-acid sequence of proteins (mRNA), and the RNA which links codon sequence
 281 to amino-acid identity during translation (tRNA). Despite the varied function of these RNA species,
 282 they share a commonality in that they are transcribed from DNA via the action of RNA polymerase.
 283 In the coming paragraphs, we will consider the synthesis of RNA as a rate limiting step in bacterial division by estimating how many RNA polymerases must be present to synthesize all necessary rRNA, mRNA, and tRNA.

286 rRNA

287 We begin with an estimation of the number of RNA polymerases needed to synthesize the rRNA
 288 that serve as catalytic and structural elements of the ribosome. Each ribosome contains three rRNA
 289 molecules of lengths 120, 1542, and 2904 nucleotides (BNID: 108093, *Milo et al. (2010)*), meaning
 290 each ribosome contains \approx 4500 nucleotides. As the *E. coli* RNA polymerase transcribes DNA to
 291 RNA at a rate of \approx 40 nucleotides per second (BNID: 101904, *Milo et al. (2010)*), it takes a single RNA
 292 polymerase \approx 100 s to synthesize the RNA needed to form a single functional ribosome. Therefore,
 293 in a 5000 s division time, a single RNA polymerase transcribing rRNA at a time would result in only
 294 \approx 50 functional ribosomal rRNA units – far below the observed number of \approx 10^4 ribosomes per cell.

295 Of course, there can be more than one RNA polymerase transcribing the rRNA genes at any given time. To elucidate the *maximum* number of rRNA units that can be synthesized given a single
 296 copy of each rRNA gene, we will consider a hypothesis in which the rRNA operon is completely tiled
 297 with RNA polymerase. *In vivo* measurements of the kinetics of rRNA transcription have revealed
 298 that RNA polymerases are loaded onto the promoter of an rRNA gene at a rate of \approx 1 per second
 299 (BNID: 111997; 102362, *Milo et al. (2010)*). If RNA polymerases are being constantly loaded on
 300 to the rRNA genes at this rate, then we can assume that \approx 1 functional rRNA unit is synthesized
 301 per second. With a 5000 second division time, this hypothesis leads to a maximal value of 5000
 302 functional rRNA units, still undershooting the observed number of 10^4 ribosomes per cell.

303 *E. coli* has evolved a clever mechanism to surpass this kinetic limit for the rate of rRNA production. Rather than having only one copy of each rRNA gene, *E. coli* has seven copies of the operon
 304 (BIND: 100352, *Milo et al. (2010)*) four of which are localized directly adjacent to the origin of replication (*Birnbaum and Kaplan, 1971*). As fast growth also implies an increased gene dosage due to
 305 paralellized chromosomal replication, the total number of rRNA genes can be on the order of \approx 10 – 70 copies at moderate to fast growth rates (*Stevenson and Schmidt, 2004*). Using our standard
 306 time scale of a 5000 second division time, we can make the lower-bound estimate that the typical
 307 cell will have 7 copies of the rRNA operon. Synthesizing one functional rRNA unit per second per
 308 rRNA operon, a total of 4×10^4 rRNA units can be synthesized, comfortably above the observed
 309 number of ribosomes per cell.

310 How many RNA polymerases are then needed to constantly transcribe 7 copies of the rRNA

315 genes? We approach this estimate by considering the maximum number of RNA polymerases tiled
 316 along the rRNA genes with a loading rate of 1 per second and a transcription rate of 40 nucleotides
 317 per second. Considering that a RNA polymerase has a physical footprint of approximately 40 nu-
 318 cleotides (BNID: 107873, *Milo et al. (2010)*), we can expect ≈ 1 RNA polymerase per 80 nucleotides.
 319 With a total length of ≈ 4500 nucleotides per operon and 7 operons per cell, the maximum number
 320 of RNA polymerases that can be transcribing rRNA at any given time is ≈ 400 . As we will see in the
 321 coming sections, the synthesis of rRNA is the dominant requirement of the RNA polymerase pool.

322 mRNA

323 To form a functional protein, all protein coding genes must first be transcribed from DNA to form
 324 an mRNA molecule. While each protein requires an mRNA blueprint, many copies of the protein
 325 can be synthesized from a single mRNA. Factors such as strength of the ribosomal binding site,
 326 mRNA stability, and rare codon usage frequency dictate the number of proteins that can be made
 327 from a single mRNA, with yields ranging from 10^1 to 10^4 (BNID: 104186; 100196; 106254, *Milo et al.*
 328 (*2010*)). Computing the geometric mean of this range yields ≈ 1000 proteins synthesized per mRNA,
 329 a value that agrees with experimental measurements of the number of proteins per cell ($\approx 3 \times 10^6$,
 330 BNID: 100088, *Milo et al. (2010)*) and total number of mRNA per cell ($\approx 3 \times 10^3$, BNID: 100064, *Milo*
 331 *et al. (2010)*).

332 This estimation captures the *steady-state* mRNA copy number, meaning that at any given time,
 333 there will exist approximately 3000 unique mRNA molecules. To determine the *total* number of
 334 mRNA that need to be synthesized over the cell's lifetime, we must consider degradation of the
 335 mRNA. In most bacteria, mRNAs are rather unstable with life times on the order of several minutes
 336 (BNID: 104324; 106253; 111927; 111998, *Milo et al. (2010)*). For convenience, we assume that the
 337 typical mRNA in our cell of interest has a typical lifetime of ≈ 300 seconds. Using this value, we
 338 can determine the total mRNA production rate to maintain a steady-state copy number of 3000
 339 mRNA per cell. While we direct the reader to the appendix for a more detailed discussion of mRNA
 340 transcriptional dynamics, we state here that the total mRNA production rate must be on the order
 341 of ≈ 15 mRNA per second. In *E. coli*, the average protein is ≈ 300 amino acids in length (BNID:
 342 108986; *Milo et al. (2010)*), meaning that the corresponding mRNA is ≈ 900 nucleotides which we
 343 will further approximate as ≈ 1000 nucleotides to account for the non-protein coding regions on
 344 the 5' and 3' ends. This means that the cell must have enough RNA polymerase molecules about
 345 to sustain a transcription rate of $\approx 1.5 \times 10^4$ nucleotides per second. Knowing that a single RNA
 346 polymerase polymerizes RNA at a clip of 40 nucleotides per second, we arrive at a comfortable
 347 estimate of ≈ 250 RNA polymerase complexes needed to satisfy the mRNA demands of the cell. It
 348 is worth noting that this number is approximately half of that required to synthesize enough rRNA,
 349 as we saw in the previous section. We find this to be a striking result as these 250 RNA polymerase
 350 molecules are responsible for the transcription of the ≈ 4000 protein coding genes that are not
 351 ribosome associated.

352 tRNA

353 The final class of RNA molecules worthy of quantitative consideration is the the pool of tRNAs
 354 used during translation to map codon sequence to amino acid identity. Unlike mRNA or rRNA,
 355 each individual tRNA is remarkably short, ranging from 70 to 95 nucleotides each (BNID: 109645;
 356 102340, *Milo et al. (2010)*). What they lack in length, they make up for in abundance. There are
 357 approximately ≈ 3000 tRNA molecules present for each of the 20 amino acids (BNID: 105280, *Milo*
 358 *et al. (2010)*), although the precise copy number is dependent on the identity of the ligated amino
 359 acid. Using these values, we make the estimate that $\approx 5 \times 10^6$ nucleotides are sequestered in tRNA
 360 per cell. Unlike mRNA, tRNA is remarkably stable with typical lifetimes *in vivo* on the order of ≈ 48
 361 hours (*Abelson et al., 1974; Svennningsen et al., 2017*) – well beyond the timescale of division. Once
 362 again using our rule-of-thumb for the rate of transcription to be 40 nucleotides per second and
 363 assuming a division time of ≈ 5000 seconds, we arrive at an estimate of ≈ 20 RNA polymerases

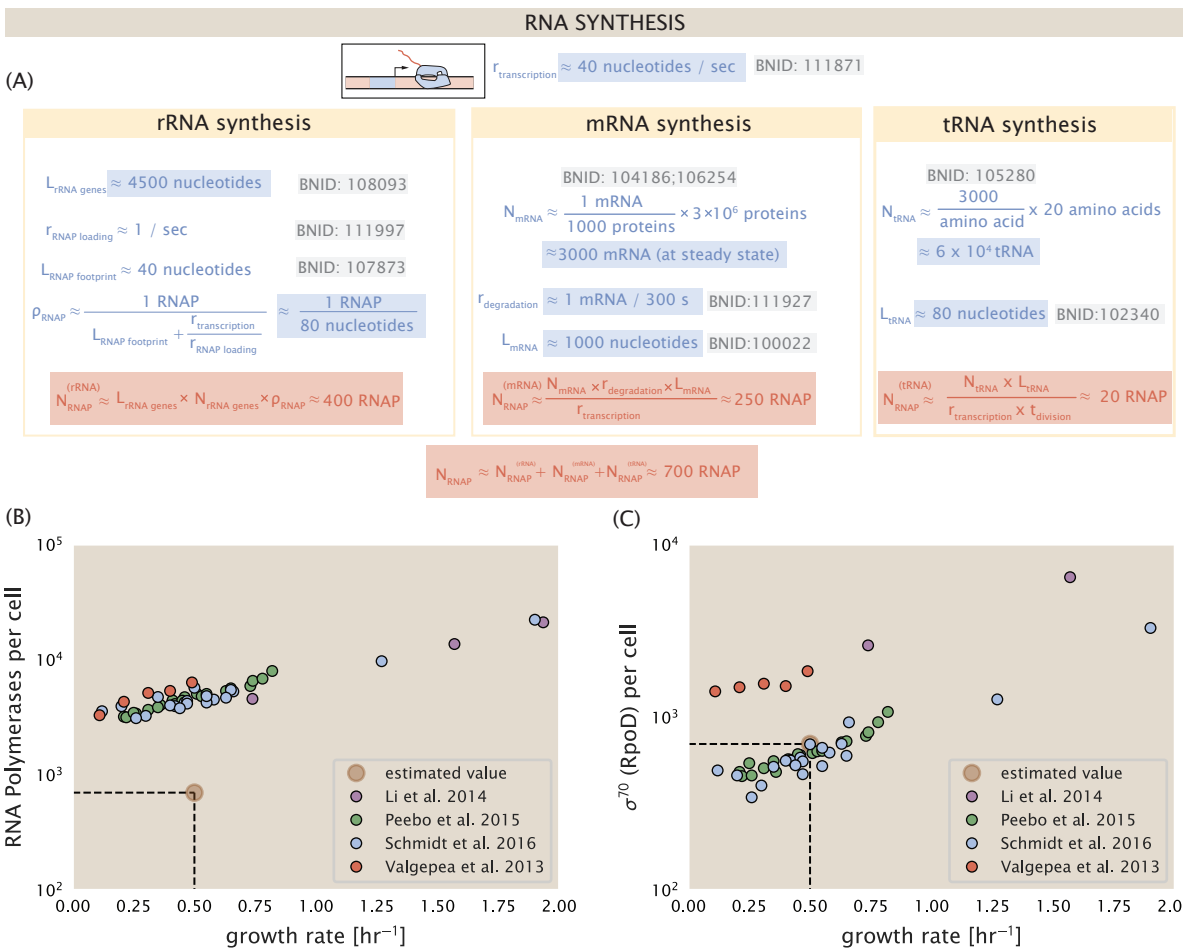


Figure 5. Estimation of the RNA polymerase demand and comparison with experimental data. (A)

Estimations for the number of RNA polymerase needed to synthesize sufficient quantities of rRNA, mRNA, and tRNA from left to right, respectively. Bionumber Identifiers (BNIDs) are provided for key quantities used in the estimates. (B) The RNA polymerase core enzyme copy number as a function of growth rate. Colored points correspond to the average number RNA polymerase core enzymes that could be formed given a subunit stoichiometry of $[RpoA]_2[RpoC][RpoB]$. (C) The abundance of σ^{70} as a function of growth rate. Estimated value for the number of RNAP is shown in (B) and (C) as a translucent brown point at a growth rate of 0.5 hr^{-1} .

364 to synthesize enough tRNA. This requirement pales in comparison to the number of polymerases
 365 needed to generate the rRNA and mRNA pools and can be neglected as a significant transcriptional
 366 burden.

367 RNA Polymerase and σ -factor Abundance

368 These estimates, summarized in **Figure 5 (A)**, reveal that synthesis of rRNA and mRNA are the domi-
 369 nant RNA species synthesized by RNA polymerase, suggesting the need for ≈ 700 RNA polymerases
 370 per cell. As is revealed in **Figure 5 (B)**, this estimate is about an order of magnitude below the ob-
 371 served number of RNA polymerase complexes per cell ($\approx 5000 - 7000$). The disagreement between
 372 the estimated number of RNA polymerases and these observations are at least consistent with
 373 recent literature revealing that $\approx 80\%$ of RNA polymerases in *E. coli* are not transcriptionally active
 374 (*Patrick et al., 2015*). Our estimate ignores the possibility that some fraction is only nonspecifically
 375 bound to DNA, as well as the obstacles that RNA polymerase and DNA polymerase present for each
 376 other as they move along the DNA (*Finkelstein and Greene, 2013*).

377 In addition, it is also vital to consider the role of σ -factors which help RNA polymerase identify

378 and bind to transcriptional start sites (*Browning and Busby, 2016*). Here we consider σ^{70} (RpoD)
 379 which is the dominant "general-purpose" σ -factor in *E. coli*. While initially thought of as being solely
 380 involved in transcriptional initiation, the past two decades of single-molecule work has revealed
 381 a more multipurpose role for σ^{70} including facilitating transcriptional elongation (*Kapanidis et al., 2005; Goldman et al., 2015; Perdue and Roberts, 2011; Mooney and Landick, 2003; Mooney et al., 2005*). **Figure 5** (B) is suggestive of such a role as the number of σ^{70} proteins per cell is in close
 382 agreement with our estimate of the number of transcriptional complexes needed.
 383

384 While these estimates and comparison with experimental data reveal an interesting dynamic
 385 at play between the transcriptional demand and copy numbers of the corresponding machinery,
 386 these findings illustrate that transcription cannot be the rate limiting step in bacterial division. **Fig-**
 387 **ure 5** (A) reveals that the availability of RNA polymerase is not a limiting factor for cell division as the
 388 cell always has an apparent ~ 10 -fold excess than needed. Furthermore, if more transcriptional
 389 activity was needed to satisfy the cellular requirements, more σ^{70} -factors could be expressed to
 390 utilize a larger fraction of the RNA polymerase pool.
 391

392 Protein synthesis

393 Lastly, we turn our attention to the process of translation. So far in our estimates there have been
 394 little to suggest any apparent limit on the cell's ability to produce the required number protein
 395 species. Even in our example of *E. coli* grown under different carbohydrate sources (**Figure 2(B)**),
 396 cells are able to utilize alternative carbon sources by inducing the expression of additional mem-
 397 brane transporters and enzymes. For a doubling time of 5000 seconds, *E. coli* has roughly 3×10^6
 398 proteins per cell, which for an average protein of 300 aa, amounts to $\approx 10^9$ peptide bonds that must
 399 be formed. This also corresponds to the number of amino-acyl tRNA that are used, with the pool
 400 of tRNA continuously recharged with new amino acids by tRNA synthetases. At a rate of charging
 401 of about 20 amino-acyl tRNA per second (BNID: 105279, *Milo et al. (2010)*), we find that cells have
 402 more than sufficient tRNA synthetases to meet the demand of ribosomes during protein synthesis
 403 (**Figure 6(A)**).

404 If we consider an elongation rate of ≈ 15 peptide bonds per second (BNID: 114271, *Milo et al. (2010); Dai et al. (2016)*), the formation of $\approx 10^9$ peptide bonds would require 1.5×10^4 ribosomes at
 405 a growth rate of 0.5 hr^{-1} . This is indeed consistent with the experimental data shown in **Figure 6(B)**.
 406 However, in view of our earlier estimate on rRNA, which suggest that rRNA operons need to be
 407 nearly packed with transcribing RNA polymerase even at relatively slow growth, there is a possi-
 408 bility that ribosomes might limit growth. While the transcriptional demand for ribosomal proteins
 409 will not be nearly as high as rRNA genes, other ribosomal proteins like the translation elongation
 410 factor EF-Tu is the most highly expressed protein and is present in two copies on the chromosome.
 411 Experimentally, consecutive deletion of rRNA operons showed a significant reduction in growth
 412 rate in rich media when cells had only 3 or less (*Levin et al., 2017*).
 413

414 We can begin to gain some intuition into how translation, or ribosomes more specifically, might
 415 limit growth by noting that the total number of peptide bonds generated as the cell doubles, N_{aa} ,
 416 which we used in our calculation above, will be given by, $\tau \cdot r_t \cdot R$. Here, τ refers to the doubling
 417 time of the cell under steady-state growth, r_t is the maximum translation elongation rate, and R is
 418 the average number of ribosomes per cell. With the growth rate related to the cell doubling time
 419 by $\lambda = \ln(2)/\tau$, we can write the translation-limited growth rate as,

$$\lambda_{\text{translation-limited}} = \frac{\ln(2) \cdot r_t \cdot R}{N_{aa}}. \quad (1)$$

420 Alternatively, since N_{aa} is related to the total protein mass through the molecular weight of each
 421 protein, we can also consider the growth rate in terms of ribosomal mass fraction. By making the
 422 approximation that an average amino acid has a molecular weight of 110 Da (see **Figure 7(A)**), we

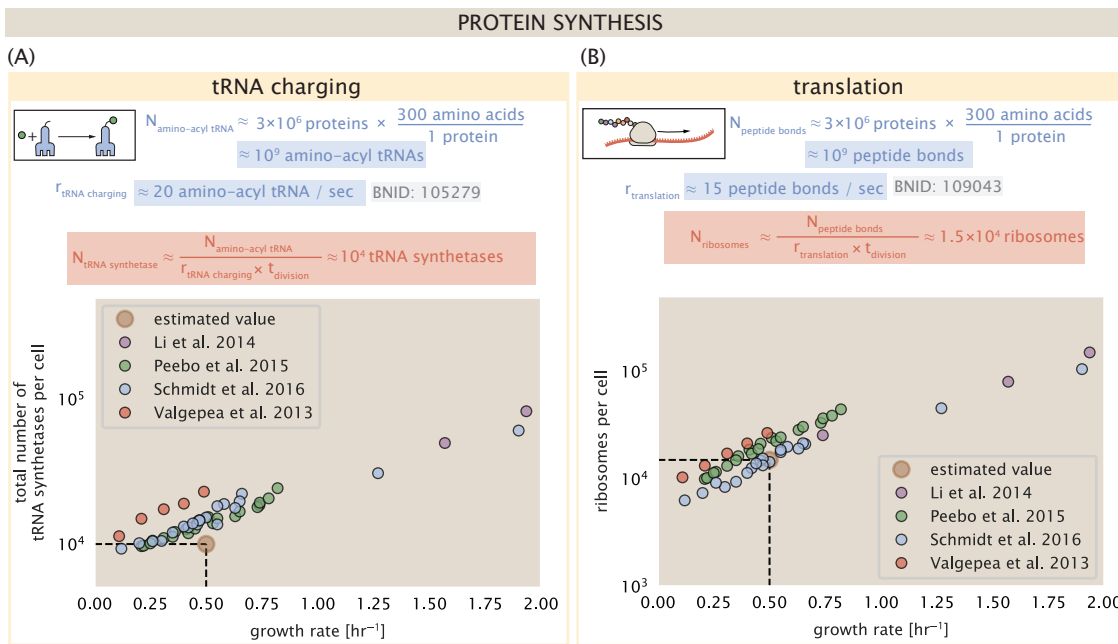


Figure 6. Estimation of the required tRNA synthetases and ribosomes. (A) Estimation for the number of tRNA synthetases that will supply the required amino acid demand. The sum of all tRNA synthetases copy numbers are plotted as a function of growth rate ([ArgS], [CysS], [GlnS], [GltX], [IleS], [LeuS], [ValS], [AlaS]₂, [AsnS]₂, [AspS]₂, [TyrS]₂, [TrpS]₂, [ThrS]₂, [SerS]₂, [ProS]₂, [PheS]₂[PheT]₂, [MetG]₂, [LysS]₂, [HisS]₂, [GlyS]₂[GlyQ]₂). (B) Estimation for the number of ribosomes required to synthesize all proteins in the cell. The average abundance of ribosomes is plotted as a function of growth rate. Our estimated values are shown for a growth rate of 0.5 hr⁻¹.

423 can rewrite the growth rate as,

$$\lambda_{\text{translation-limited}} \approx \frac{\ln(2) \cdot r_t}{L_R} \Phi_R, \quad (2)$$

424 where L_R is the total length in amino acids that make up a ribosome, and Φ_R is the ribosomal
425 mass fraction. This is plotted as a function of ribosomal fraction Φ_R in **Figure 7(A)**, where we take
426 $L_R \approx 7459$ aa, corresponding to the length in amino acids for all ribosomal subunits of the 50S and
427 30S complex. This formulation assumes that the cell can also transcribe the required amount of
428 rRNA, allowing us to consider the inherent limit on growth set by the ribosome.

429 Perhaps the first thing to notice is that there is a maximum growth rate at about $\lambda \approx 6 \text{ hr}^{-1}$,
430 or doubling time of about 7 minutes (dashed line). This growth rate can be viewed as an inherent
431 maximum rate due to the need for the cell to double the cell's entire ribosomal mass. Interestingly,
432 this limit is independent of the absolute number of ribosomes, but rather is simply given by time
433 to translate an entire ribosome, L_R/r_t . As shown in **Figure 7(B)**, we can reconcile this with the ob-
434 servation that in order to double the average number of ribosomes, each ribosome must produce
435 a second ribosome. This is a process that cannot be parallelized.

436 For reasonable values of Φ_R , in the range of about 0.1 - 0.3 (*Scott et al., 2010*), the maximum
437 growth rate is in line with experimentally reported growth rates around 0.5 - 2 hr⁻¹. Here we have
438 implicitly assumed that translation proceeds randomly, without preference between ribosomal or
439 non-ribosomal mRNA, which appears reasonable. Importantly, in order for a cell to scale this limit
440 set by Φ_R the cell must increase its ribosomal abundance, either by synthesizing more ribosomes
441 or reducing the fraction of non-ribosomal proteins.

442 While it is common for bacteria to decrease their ribosomal abundance in poorer nutrient con-
443 ditions (*Scott et al. (2010); Liebermeister et al. (2014)*), this does not decrease to zero. From the
444 perspective of a bacterium dealing with uncertain nutrient conditions, there is likely a benefit for

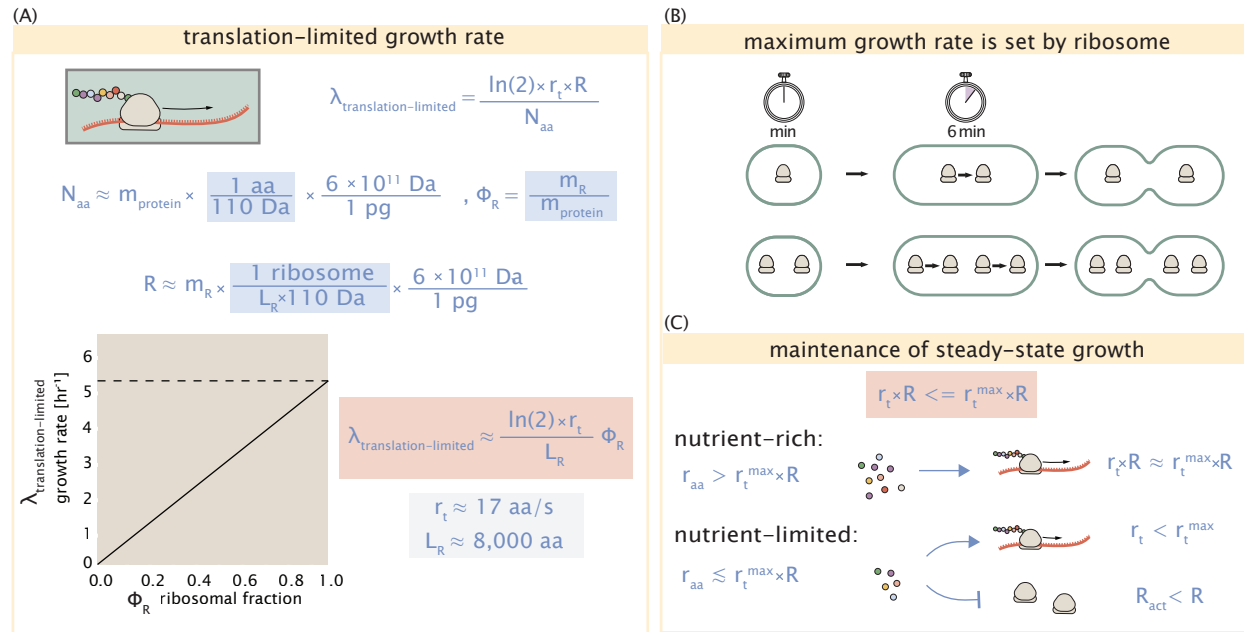


Figure 7. Translation-limited growth rate. (A) Here we consider the translation-limited growth as a function of ribosomal fraction. By mass balance, the time required to double the entire proteome (N_{aa} / r_t) sets the translation-limited growth rate, $\lambda_{\text{translation-limited}}$. Here N_{aa} is effectively the number of peptide bonds that must be translated, r_t is the translation elongation rate, and R is the number of ribosomes. This can also be re-written in terms of the ribosomal mass fraction $\Phi_R = m_R / m_{\text{protein}}$, where m_R is the total ribosomal mass and m_{protein} is the mass of all proteins in the cell. L_R refers to the summed length of the ribosome in amino acids. $\lambda_{\text{translation-limited}}$ is plotted as a function of Φ_R (solid line). (B) The dashed line in part (A) identifies a maximum growth rate that is set by the ribosome. Specifically, this growth rate corresponds to the time required to translate an entire ribosome, L_R / r_t . This is a result that is independent of the number of ribosomes in the cell as shown schematically here. (C) Schematic showing translation-specific requirements for maintenance of steady-state growth. In a nutrient rich environment, amino acid supply r_{aa} is sufficiently in excess of demand by ribosomes translating at their maximal rate. In poorer nutrient conditions, reduced amino acid supply r_{aa} will decrease the rate of elongation. In a regime where $r_{\text{aa}} < r_t \cdot R$, the number of actively translating ribosomes will need to be reduced in order to maintain steady-state growth.

445 the cell to maintain some relative fraction of ribosomes to support rapid growth as nutrient condi-
 446 tions improve. However, if we consider a scenario where nutrient conditions become poorer and
 447 poorer, there will be a regime where ribosomes are in excess of the nutrient supply. If the cell is
 448 to maintain steady-state growth, it will need to attenuate its translational activity since ribosomes
 449 would otherwise exhaust their supply of amino acids and bring cell growth to a halt (**Figure 7(C)**).
 450 In the next section we will consider this more specifically for *E. coli*, which has been shown to main-
 451 tain a relatively high elongation rate even in stationary phase (≈ 8 aa/s, **Dai et al. (2016)**) where cell
 452 growth is minimal.

453 **Multiple replication forks bias ribosome abundance.**

454 *E. coli* cells grow by an adder mechanism, whereby cells add a constant volume with each cell di-
 455 vision (**Taheri-Araghi et al., 2015**). In conjunction with this, additional rounds of DNA replication
 456 are triggered when cells reach a critical volume per origin of replication (**Figure 8(A)**). This leads to
 457 the classically-described exponential increase in cell size with growth rate **Schaechter et al. (1958)**;
 458 **Si et al. (2017, 2019)**. In the context of maximizing growth rate, it is notable that the majority of
 459 ribosomal proteins and rRNA operons are found closer to the DNA origin. Given the necessity of
 460 increasing the effective number of rRNA operons at faster growth rates, this raises the possibil-
 461 ity that the observed size scaling and increase in chromosomal equivalents might simply be as a
 462 means for the cell to tune biosynthetic rates according to its physiological state.

463 While an increase in transcription has been observed for genes near the origin in rapidly grow-
 464 ing *E. coli* (**Scholz et al., 2019**), we were unaware of such characterization at the proteomic level.
 465 In order to test whether such a skew in expression exists at the protein level at faster growth, we
 466 calculated a running boxcar average of protein copy number as a function of their transcrip-
 467 tional start sites. While absolute protein copy numbers vary substantially across the chromosome, we
 468 indeed observe a bias in expression under faster growth conditions (**Figure 8(B)**, showing the result
 469 using a 0.5 kb averaging window). The dramatic change in protein copy number near the origin
 470 mainly reflects the increase in ribosomal protein expression. This trend is in contrast to slower
 471 growth conditions where the average copy number is more uniform across the length of the chro-
 472 mosome.

473 If ribosomal genes (rRNA and ribosomal proteins) are being synthesized according to their avail-
 474 able gene dosage we can make two related hypotheses about how ribosomal abundance should
 475 vary with chromosomal content. The first is that the ribosomal protein fraction should increase
 476 in proportion to the average ratio of DNA origins to DNA termini ($\langle \# \text{ ori} \rangle / \langle \# \text{ ter} \rangle$ ratio), which is
 477 a consequence of the skew in DNA dosage as cells grow faster. The second is that the absolute
 478 number of ribosomes should increase in proportion to the number of DNA origins ($\langle \# \text{ ori} \rangle$), since
 479 this will reflect the total gene dosage at a particular growth condition.

480 In order to test these hypotheses we considered the experimental data from **Si et al. (2017)**,
 481 which determined these parameters under nutrient-limited growth. $\langle \# \text{ ori} \rangle / \langle \# \text{ ter} \rangle$ ratio depends
 482 on how quickly chromosomes are replicated relative the cell's doubling time τ and is given by $2^{\tau_c/\tau}$.
 483 Here τ_c is the time taken to replicate the chromosome, referred to as the C period of cell division.
 484 In **Figure 8(C)** we plot τ_c versus τ that were measured, with data points in red corresponding to
 485 *E. coli* strain MG1655, and blue to strain NCM3722. In their work they also measured the total
 486 RNA to protein ratio which reflects ribosomal abundance and we show that data along with other
 487 recent measurements from **Dai et al.** Indeed we find that the ribosomal fraction increases with
 488 $\langle \# \text{ ori} \rangle / \langle \# \text{ ter} \rangle$ (**Figure 8(C)**). Across our different proteomic data sets there also appeared two
 489 distinct trends. To consider the possibility that this may reflect systematic differences in how the
 490 data was generated, we also considered recent measurements of total RNA to protein ratio across
 491 the growth rates considered, which provide an alternative measure of ribosomal abundance (RNA
 492 to protein ratio $\approx \Phi_R \times 2.1$ **Dai et al. (2016)**). While these showed a similar correlation, they were
 493 most consistent with the proteomic data from **Schmidt et al. (2016)** and **Li et al. (2014)**.

494 We can similarly estimate $\langle \# \text{ ori} \rangle$, which depends on how often replication forks are initiated

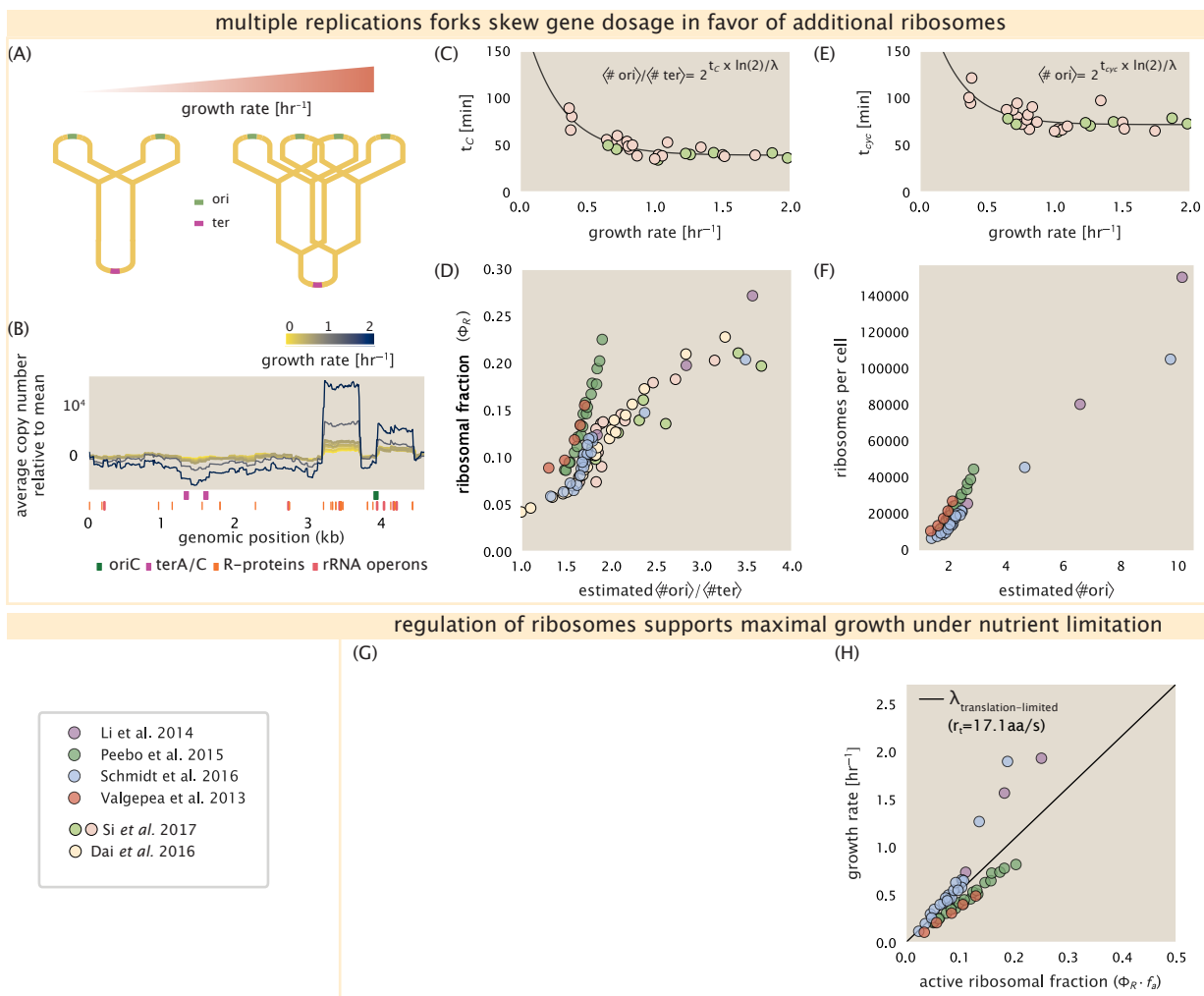


Figure 8. Multiple replication forks skew gene dosage and ribosomal content. (A) Schematic shows the expected increase in replication forks (or number of ori regions) as *E. coli* cells grow faster. (B) A running boxcar average of protein copy number is calculated for each growth condition considered by Schmidt *et al.*. A 0.5 kb averaging window was used. Protein copy numbers are reported relative to their condition-specific means in order to center all data sets. (C) and (E) show experimental data from Si *et al.* (2017). Solid lines show fits to the data, which were used to estimate $\langle \# \text{ori} \rangle / \langle \# \text{ter} \rangle$ and $\langle \# \text{ori} \rangle$ [NB: to note fit equations]. Red data points correspond to measurements in strain MG1655, while light green points are for strain NCM3722. (D) Plot compares our estimate of $\langle \# \text{ori} \rangle / \langle \# \text{ter} \rangle$ to the experimental measurements of ribosomal abundance. Ribosomal fraction was approximated from the RNA/protein ratios of Dai *et al.* (2016) (yellow) and Si *et al.* (2017) (light red and light green) by the conversion $\text{RNA/protein ratio} \approx \Phi_R \cdot 2.1$. (F) plots the ribosome copy number estimated from the proteomic data against our estimate of $\langle \# \text{ori} \rangle$. (G) [in progress], (H) Experimental data from Dai *et al.* are used to estimate the fraction of actively translating ribosomes. The solid line represents the translation-limited growth rate for ribosomes elongating at 17.1 aa/s.

495 per cell cycle. This is given by the number of overlapping cell cycles, $2^{\tau_{cyc}/\tau}$, where τ_{cyc} , refers to
 496 the total time of chromosome replication and cell division. **Figure 8(E)** shows the associated data
 497 from Si *et al.*, which we use to estimate $\langle \# \text{ori} \rangle$ for each growth condition of the proteomic data. In
 498 agreement with our expectations, we find a strong correlation between the ribosome copy number
 499 and estimated $\langle \# \text{ori} \rangle$ (**Figure 8(F)**).

500 [NB: to do. 1) slow growth regime, 2) putting it all together ; cells appear to grow near the
 501 translation-limited rate ($r_t = 17 \text{aa/s}$) across all growth conditions. Need to provide some rational-
 502 ization for points above line.]

503 [NB: Titration of the cellular ppGpp concentration invoked similar proteomic changes to those
 504 observed under nutrient limitation (**Zhu and Dai, 2019**). In light of our hypothesis that such changes
 505 to the proteome are intimately linked to the details of DNA replication, it was recently shown that
 506 both the $\langle \# \text{ori} \rangle / \langle \# \text{ter} \rangle$ and cell size lost their growth rate dependent scaling in a ppGpp null strain.
 507 Rather, cells exhibit a $\langle \# \text{ori} \rangle / \langle \# \text{ter} \rangle$ closer to 4 and cell size more consistent with a fast growth state
 508 (**Fernández-Coll et al., 2020**). This supports the possibility that in addition to coordinating ribosome
 509 activity, (p)ppGpp signaling may be acting to coordinate other cellular processes in accordance
 510 with nutrient conditions and biosynthetic demand. From this perspective, the increase in the rate
 511 of DNA initiation and associated increase in cell size may be viewed as a way for the cell to vary its
 512 proteomic composition and biosynthetic capacity according to its available nutrient conditions.]

513 References

- 514 Abelson, H., Johnson, L., Penman, S., and Green, H. (1974). Changes in RNA in relation to growth of the fibroblast:
 515 II. The lifetime of mRNA, rRNA, and tRNA in resting and growing cells. *Cell*, 1(4):161–165.
- 516 Adelberg, G., Towbin, B. D., Rothschild, D., Dekel, E., Bren, A., and Alon, U. (2014). Hierarchy of non-glucose
 517 sugars in Escherichia coli. *BMC Systems Biology*, 8(1):133.
- 518 Antonenko, Y. N., Pohl, P., and Denisov, G. A. (1997). Permeation of ammonia across bilayer lipid membranes
 519 studied by ammonium ion selective microelectrodes. *Biophysical Journal*, 72(5):2187–2195.
- 520 Ason, B., Bertram, J. G., Hingorani, M. M., Beechem, J. M., O'Donnell, M., Goodman, M. F., and Bloom, L. B.
 521 (2000). A Model for *Escherichia coli* DNA Polymerase III Holoenzyme Assembly at Primer/Template Ends:
 522 DNA Triggers A Change In Binding Specificity of the γ Complex Clamp Loader. *Journal of Biological Chemistry*,
 523 275(4):3006–3015.
- 524 Assentoft, M., Kaptan, S., Schneider, H.-P., Deitmer, J. W., de Groot, B. L., and MacAulay, N. (2016). Aquaporin 4
 525 as a NH3 Channel. *Journal of Biological Chemistry*, 291(36):19184–19195.
- 526 Bauer, S. and Ziv, E. (1976). Dense growth of aerobic bacteria in a bench-scale fermentor. *Biotechnology and
 527 Bioengineering*, 18(1):81–94. _eprint: <https://onlinelibrary.wiley.com/doi/10.1002/bit.260180107>.
- 528 Belliveau, N. M., Barnes, S. L., Ireland, W. T., Jones, D. L., Sweredoski, M. J., Moradian, A., Hess, S., Kinney, J. B.,
 529 and Phillips, R. (2018). Systematic approach for dissecting the molecular mechanisms of transcriptional
 530 regulation in bacteria. *Proceedings of the National Academy of Sciences*, 115(21):E4796–E4805.
- 531 Birnbaum, L. S. and Kaplan, S. (1971). Localization of a Portion of the Ribosomal RNA Genes in *Escherichia coli*.
 532 *Proceedings of the National Academy of Sciences*, 68(5):925–929.
- 533 Booth, I. R., Mitchell, W. J., and Hamilton, W. A. (1979). Quantitative analysis of proton-linked transport systems.
 534 The lactose permease of *Escherichia coli*. *Biochemical Journal*, 182(3):687–696.
- 535 Bremer, H. and Dennis, P. P. (2008). Modulation of Chemical Composition and Other Parameters of the Cell at
 536 Different Exponential Growth Rates. *EcoSal Plus*, 3(1).
- 537 Browning, D. F. and Busby, S. J. W. (2016). Local and global regulation of transcription initiation in bacteria.
 538 *Nature Reviews Microbiology*, 14(10):638–650.
- 539 Dai, X., Zhu, M., Warren, M., Balakrishnan, R., Patsalo, V., Okano, H., Williamson, J. R., Fredrick, K., Wang, Y.-P.,
 540 and Hwa, T. (2016). Reduction of translating ribosomes enables *Escherichia coli* to maintain elongation rates
 541 during slow growth. *Nature Microbiology*, 2(2):16231.

- 542 Escalante, A., Salinas Cervantes, A., Gosset, G., and Bolívar, F. (2012). Current knowledge of the Escherichia coli
 543 phosphoenolpyruvate-carbohydrate phosphotransferase system: Peculiarities of regulation and impact on
 544 growth and product formation. *Applied Microbiology and Biotechnology*, 94(6):1483–1494.
- 545 Feist, A. M., Henry, C. S., Reed, J. L., Krummenacker, M., Joyce, A. R., Karp, P. D., Broadbelt, L. J., Hatzimanikatis,
 546 V., and Palsson, B. Ø. (2007). A genome-scale metabolic reconstruction for Escherichia coli K-12 MG1655 that
 547 accounts for 1260 ORFs and thermodynamic information. *Molecular Systems Biology*, 3(1):121.
- 548 Fernández-Coll, L., Maciąg-Dorszynska, M., Tailor, K., Vadia, S., Levin, P. A., Szalewska-Palasz, A., Cashel, M.,
 549 and Dunny, G. M. (2020). The Absence of (p)ppGpp Renders Initiation of Escherichia coli Chromosomal DNA
 550 Synthesis Independent of Growth Rates. *mBio*, 11(2):45.
- 551 Fijalkowska, I. J., Schaaper, R. M., and Jonczyk, P. (2012). DNA replication fidelity in Escherichia coli: A multi-DNA
 552 polymerase affair. *FEMS Microbiology Reviews*, 36(6):1105–1121.
- 553 Finkelstein, I. J. and Greene, E. C. (2013). Molecular Traffic Jams on DNA. *Annual Review of Biophysics*, 42(1):241–
 554 263.
- 555 Gama-Castro, S., Salgado, H., Santos-Zavaleta, A., Ledezma-Tejeida, D., Muñiz-Rascado, L., García-Sotelo, J. S.,
 556 Alquicira-Hernández, K., Martínez-Flores, I., Pannier, L., Castro-Mondragón, J. A., Medina-Rivera, A., Solano-
 557 Lira, H., Bonavides-Martínez, C., Pérez-Rueda, E., Alquicira-Hernández, S., Porrón-Sotelo, L., López-Fuentes,
 558 A., Hernández-Koutoucheva, A., Moral-Chávez, V. D., Rinaldi, F., and Collado-Vides, J. (2016). RegulonDB
 559 version 9.0: High-level integration of gene regulation, coexpression, motif clustering and beyond. *Nucleic
 560 Acids Research*, 44(D1):D133–D143.
- 561 Ge, J., Yu, G., Ator, M. A., and Stubbe, J. (2003). Pre-Steady-State and Steady-State Kinetic Analysis of *E. coli* Class
 562 I Ribonucleotide Reductase. *Biochemistry*, 42(34):10071–10083.
- 563 Goldman, S. R., Nair, N. U., Wells, C. D., Nickels, B. E., and Hochschild, A. (2015). The primary σ factor in *Es-*
 564 *cherichia coli* can access the transcription elongation complex from solution *in vivo*. *eLife*, 4:e10514.
- 565 Harris, R. M., Webb, D. C., Howitt, S. M., and Cox, G. B. (2001). Characterization of PitA and PitB from *Escherichia*
 566 *coli*. *Journal of Bacteriology*, 183(17):5008–5014.
- 567 Heldal, M., Norland, S., and Tumyr, O. (1985). X-ray microanalytic method for measurement of dry matter and
 568 elemental content of individual bacteria. *Applied and Environmental Microbiology*, 50(5):1251–1257.
- 569 Ireland, W. T., Beeler, S. M., Flores-Bautista, E., Belliveau, N. M., Sweredoski, M. J., Moradian, A., Kinney, J. B.,
 570 and Phillips, R. (2020). Deciphering the regulatory genome of *Escherichia coli*, one hundred promoters at a
 571 time. *bioRxiv*.
- 572 Jacob, F. and Monod, J. (1961). Genetic regulatory mechanisms in the synthesis of proteins. *Journal of Molecular
 573 Biology*, 3(3):318–356.
- 574 Jensen, R. B., Wang, S. C., and Shapiro, L. (2001). A moving DNA replication factory in *Caulobacter crescentus*.
 575 *The EMBO journal*, 20(17):4952–4963.
- 576 Jun, S., Si, F., Pugatch, R., and Scott, M. (2018). Fundamental principles in bacterial physiology - history, recent
 577 progress, and the future with focus on cell size control: A review. *Reports on Progress in Physics*, 81(5):056601.
- 578 Kapanidis, A. N., Margeat, E., Laurence, T. A., Doose, S., Ho, S. O., Mukhopadhyay, J., Kortkhonjia, E., Mekler, V.,
 579 Ebright, R. H., and Weiss, S. (2005). Retention of Transcription Initiation Factor Σ 70 in Transcription Elonga-
 580 tion: Single-Molecule Analysis. *Molecular Cell*, 20(3):347–356.
- 581 Khademi, S., O'Connell, J., Remis, J., Robles-Colmenares, Y., Miercke, L.J. W., and Stroud, R. M. (2004). Mechanism
 582 of Ammonia Transport by Amt/MEP/Rh: Structure of AmtB at 1.35 Å. *Science*, 305(5690):1587–1594.
- 583 Levin, B. R., McCall, I. C., Perrot, V., Weiss, H., Ovesepian, A., and Baquero, F. (2017). A Numbers Game: Ribosome
 584 Densities, Bacterial Growth, and Antibiotic-Mediated Stasis and Death. *mBio*, 8(1).
- 585 Li, G.-W., Burkhardt, D., Gross, C., and Weissman, J. S. (2014). Quantifying absolute protein synthesis rates
 586 reveals principles underlying allocation of cellular resources. *Cell*, 157(3):624–635.
- 587 Lieberman, W., Noor, E., Flamholz, A., Davidi, D., Bernhardt, J., and Milo, R. (2014). Visual account of protein
 588 investment in cellular functions. *Proceedings of the National Academy of Sciences*, 111(23):8488–8493.

- 589 Liu, M., Durfee, T., Cabrera, J. E., Zhao, K., Jin, D. J., and Blattner, F. R. (2005). Global Transcriptional Programs
 590 Reveal a Carbon Source Foraging Strategy by *Escherichia coli*. *Journal of Biological Chemistry*, 280(16):15921–
 591 15927.
- 592 Milo, R., Jorgensen, P., Moran, U., Weber, G., and Springer, M. (2010). BioNumbers—the database of key num-
 593 bers in molecular and cell biology. *Nucleic Acids Research*, 38(suppl_1):D750–D753.
- 594 Monod, J. (1947). The phenomenon of enzymatic adaptation and its bearings on problems of genetics and
 595 cellular differentiation. *Growth Symposium*, 9:223–289.
- 596 Mooney, R. A., Darst, S. A., and Landick, R. (2005). Sigma and RNA Polymerase: An On-Again, Off-Again Rela-
 597 tionship? *Molecular Cell*, 20(3):335–345.
- 598 Mooney, R. A. and Landick, R. (2003). Tethering $\Sigma 70$ to RNA polymerase reveals high *in vivo* activity of σ factors
 599 and $\Sigma 70$ -dependent pausing at promoter-distal locations. *Genes & Development*, 17(22):2839–2851.
- 600 Neidhardt, F. C., Ingraham, J., and Schaechter, M. (1991). *Physiology of the Bacterial Cell - A Molecular Approach*,
 601 volume 1. Elsevier.
- 602 Patrick, M., Dennis, P. P., Ehrenberg, M., and Bremer, H. (2015). Free RNA polymerase in *Escherichia coli*.
 603 *Biochimie*, 119:80–91.
- 604 Peebo, K., Valgepea, K., Maser, A., Nahku, R., Adamberg, K., and Vilu, R. (2015). Proteome reallocation in *Es-
 605 cherichia coli* with increasing specific growth rate. *Molecular BioSystems*, 11(4):1184–1193.
- 606 Perdue, S. A. and Roberts, J. W. (2011). σ^{70} -dependent Transcription Pausing in *Escherichia coli*. *Journal of
 607 Molecular Biology*, 412(5):782–792.
- 608 Phillips, R. (2018). Membranes by the Numbers. In *Physics of Biological Membranes*, pages 73–105. Springer,
 609 Cham, Cham.
- 610 Ramos, S. and Kaback, H. R. (1977). The relation between the electrochemical proton gradient and active trans-
 611 port in *Escherichia coli* membrane vesicles. *Biochemistry*, 16(5):854–859.
- 612 Rosenberg, H., Gerdes, R. G., and Chegwidden, K. (1977). Two systems for the uptake of phosphate in *Es-
 613 cherichia coli*. *Journal of Bacteriology*, 131(2):505–511.
- 614 Rudd, S. G., Valerie, N. C. K., and Helleday, T. (2016). Pathways controlling dNTP pools to maintain genome
 615 stability. *DNA Repair*, 44:193–204.
- 616 Sánchez-Romero, M. A., Molina, F., and Jiménez-Sánchez, A. (2011). Organization of ribonucleoside diphosphate
 617 reductase during multifork chromosome replication in *Escherichia coli*. *Microbiology*, 157(8):2220–2225.
- 618 Schaechter, M., Maaløe, O., and Kjeldgaard, N. O. (1958). Dependency on Medium and Temperature of Cell Size
 619 and Chemical Composition during Balanced Growth of *Salmonella typhimurium*. *Microbiology*, 19(3):592–606.
- 620 Schmidt, A., Kochanowski, K., Vedelaar, S., Ahrné, E., Volkmer, B., Callipo, L., Knoops, K., Bauer, M., Aebersold,
 621 R., and Heinemann, M. (2016). The quantitative and condition-dependent *Escherichia coli* proteome. *Nature
 622 Biotechnology*, 34(1):104–110.
- 623 Scholz, S. A., Diao, R., Wolfe, M. B., Fivenson, E. M., Lin, X. N., and Freddolino, P. L. (2019). High-Resolution
 624 Mapping of the *Escherichia coli* Chromosome Reveals Positions of High and Low Transcription. *Cell Systems*,
 625 8(3):212–225.e9.
- 626 Scott, M., Gunderson, C. W., Mateescu, E. M., Zhang, Z., and Hwa, T. (2010). Interdependence of cell growth and
 627 gene expression: origins and consequences. *Science*, 330(6007):1099–1102.
- 628 Sekowska, A., Kung, H.-F., and Danchin, A. (2000). Sulfur Metabolism in *Escherichia coli* and Related Bacteria:
 629 Facts and Fiction. *Journal of Molecular Microbiology and Biotechnology*, 2(2):34.
- 630 Si, F., Le Treut, G., Sauls, J. T., Vadia, S., Levin, P. A., and Jun, S. (2019). Mechanistic Origin of Cell-Size Control
 631 and Homeostasis in Bacteria. *Current Biology*, 29(11):1760–1770.e7.
- 632 Si, F., Li, D., Cox, S. E., Sauls, J. T., Azizi, O., Sou, C., Schwartz, A. B., Erickstad, M. J., Jun, Y., Li, X., and Jun, S. (2017).
 633 Invariance of Initiation Mass and Predictability of Cell Size in *Escherichia coli*. *Current Biology*, 27(9):1278–
 634 1287.

- 635 Sirko, A., Zatyka, M., Sadowy, E., and Hulanicka, D. (1995). Sulfate and thiosulfate transport in *Escherichia coli* K-
636 12: Evidence for a functional overlapping of sulfate- and thiosulfate-binding proteins. *Journal of Bacteriology*,
637 177(14):4134–4136.
- 638 Stasi, R., Neves, H. I., and Spira, B. (2019). Phosphate uptake by the phosphonate transport system PhnCDE.
639 *BMC Microbiology*, 19.
- 640 Stevenson, B. S. and Schmidt, T. M. (2004). Life History Implications of rRNA Gene Copy Number in *Escherichia*
641 *coli*. *Applied and Environmental Microbiology*, 70(11):6670–6677.
- 642 Svenningsen, S. L., Kongstad, M., Stenum, T. S. n., Muñoz-Gómez, A. J., and Sørensen, M. A. (2017). Transfer RNA
643 is highly unstable during early amino acid starvation in *Escherichia coli*. *Nucleic Acids Research*, 45(2):793–804.
- 644 Szenk, M., Dill, K. A., and de Graff, A. M. R. (2017). Why Do Fast-Growing Bacteria Enter Overflow Metabolism?
645 Testing the Membrane Real Estate Hypothesis. *Cell Systems*, 5(2):95–104.
- 646 Taheri-Araghi, S., Bradde, S., Sauls, J. T., Hill, N. S., Levin, P. A., Paulsson, J., Vergassola, M., and Jun, S. (2015).
647 Cell-size control and homeostasis in bacteria. - PubMed - NCBI. *Current Biology*, 25(3):385–391.
- 648 Taymaz-Nikerel, H., Borjeni, A. E., Verheijen, P. J. T., Heijnen, J. J., and van Gulik, W. M. (2010).
649 Genome-derived minimal metabolic models for *Escherichia coli* MG1655 with estimated in
650 vivo respiratory ATP stoichiometry. *Biotechnology and Bioengineering*, 107(2):369–381. _eprint:
651 <https://onlinelibrary.wiley.com/doi/pdf/10.1002/bit.22802>.
- 652 Valgepea, K., Adamberg, K., Seiman, A., and Vilu, R. (2013). *Escherichia coli* achieves faster growth by increasing
653 catalytic and translation rates of proteins. *Molecular BioSystems*, 9(9):2344.
- 654 van Heeswijk, W. C., Westerhoff, H. V., and Boogerd, F. C. (2013). Nitrogen Assimilation in *Escherichia coli*: Putting
655 Molecular Data into a Systems Perspective. *Microbiology and Molecular Biology Reviews*, 77(4):628–695.
- 656 Willsky, G. R., Bennett, R. L., and Malamy, M. H. (1973). Inorganic Phosphate Transport in *Escherichia coli*:
657 Involvement of Two Genes Which Play a Role in Alkaline Phosphatase Regulation. *Journal of Bacteriology*,
658 113(2):529–539.
- 659 Zhang, L., Jiang, W., Nan, J., Almqvist, J., and Huang, Y. (2014a). The *Escherichia coli* CysZ is a pH dependent
660 sulfate transporter that can be inhibited by sulfite. *Biochimica et Biophysica Acta (BBA) - Biomembranes*,
661 1838(7):1809–1816.
- 662 Zhang, Z., Aboulwafa, M., and Saier, M. H. (2014b). Regulation of crp gene expression by the catabolite repres-
663 sor/activator, cra, in *Escherichia coli*. *Journal of Molecular Microbiology and Biotechnology*, 24(3):135–141.
- 664 Zhu, M. and Dai, X. (2019). Growth suppression by altered (p)ppGpp levels results from non-optimal resource
665 allocation in *Escherichia coli*. *Nucleic Acids Research*, 47(9):4684–4693.